Model guided design of enhanced bi-stable controllers to effectively switch cellular states

Kaushik Raj[1], William T. Z. Wong[1], Beini Zhang[1], and Radhakrishnan Mahadevan[1,2,**]

[1]Department of Chemical Engineering and Applied Chemistry, University of Toronto, Canada
[2]Institute of Biomaterials and Bioengineering, University of Toronto, Canada
[**]Corresponding author, krishna.mahadevan@utoronto.ca

1 Abstract

Bi-stable gene regulatory motifs are found in a wide variety of natural gene regulatory networks and typically effect transcriptional switching between stable phenotypic states in cells. In synthetic gene regulatory circuits, these architectures can be used to dynamically switch between distinct metabolic states for metabolic engineering and therapeutic applications. Though it has been over two decades since the first synthetic bi-stable switch was developed, the lack of modularity and predictability of these motifs in varying environments has limited widespread application, especially since the factors that affect switching characteristics are still unclear. In this work, we develop a mathematical model describing a bi-stable gene regulatory element using mass action kinetics. Using this model and a newly developed dynamical modeling and continuity analysis framework, we identify the changes in switching characteristics shown by the bi-stable motif over a range of biologically relevant model parameter values. Interestingly, there appears to be a trade-off between the robustness of the motif - the parameter ranges over which it retains bi-stable function, and the speed at which it effects a phenotypic change. Further, using *E. coli* as a model host, we constructed a large library of transcriptional switches that show a wide range of switching speeds, to experimentally demonstrate the presence of this trade-off. The presence of this trade-off has significant implications on the design of transcriptional switches for diverse applications and could potentially explain the circuit architecture of natural transcriptional switches as well. Additionally, we anticipate that our diverse library of bi-stable switches will be valuable to effect phenotypic changes with differing switching speed requirements for metabolic engineering applications.

2 Introduction

Gene regulatory networks in cells confer them the ability to sense their environments and actuate an array of intracellular and extracellular transcription based responses such as the production of substrate assimilation machinery[1], initiating cell division[2], and fighting extracellular pathogens[3]. These networks can be decomposed into smaller sub-networks or motifs that are composed of a few parts and carry out a specific function[4]. One such motif is the bi-stable gene regulatory motif, which helps cells exhibit two

distinct stable phenotypic states in response to environmental cues. It is considered to be a primitive form of cellular memory[5], since even the transient presence of inducer molecules can effect a stable change in the state of the motif. Such motifs are realized in the native gene regulatory networks of organisms using a double-negative feedback architecture (i.e. two repressors repressing each other's transcription from inducible promoters) or a positive auto-regulatory architecture (i.e. a transcription factor that induces its own production)[5].

Inspired by the design of the naturally available lambda phage switch, the first synthetic bi-stable motif - the genetic toggle switch Figure 1 was constructed using a system of repressors that inhibit each other's transcription and is considered to be a pioneering invention in the field of synthetic biology[6]. Since its conception, it has been employed in several bio-engineering applications, including in metabolic engineering to decouple growth and production metabolic states to improve chemical production[7,8], and in therapeutic applications to detect the presence of inflammation markers[9,10]. It has also been proposed as a solution for bio-containment of engineered microbes, designed to kill cells that are outside a contained environment[11,12]. The presence of two stable steady states reduces the amount and duration of inducer required to effect a response in the switch, making it a highly valuable induction system in noisy environments to reduce cellular heterogeneity.

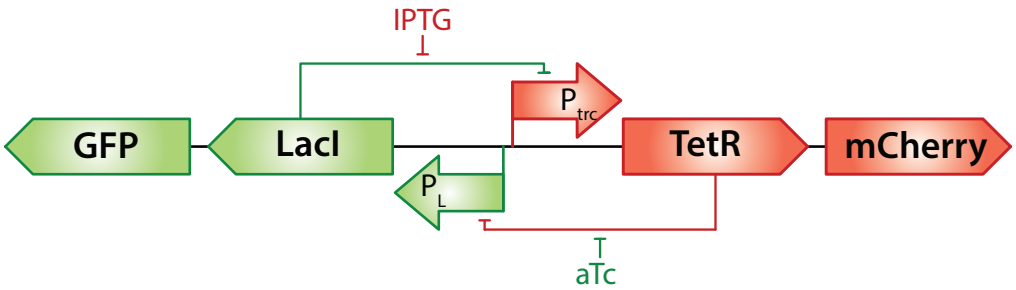

Figure 1: Genetic Toggle Switch - The genetic toggle switch constructed by Litcofsky et al[13] was selected as a base to make further modifications. This system uses the repressors LacI and TetR which mutually repress each other's production to create bi-stable gene expression.

However, despite these proof-of-concept applications, bi-stable motifs have not seen widespread use in scaled up chemical production or therapeutic applications. A major concern with employing this motif for diverse applications, is its context specificity and the lack of predictability of its function. Specifically, many versions of the switch have been shown to be bi-stable only in a narrow range of conditions, becoming mono-stable under certain conditions[6,14]. This precludes their deployment as memory elements that require transient induction. Additionally, since these switches use transcription - a relatively slow process in cells, the time taken to switch between the states can be quite large[7]. This impacts their use in metabolic engineering applications where a fast switch from growth to production stage may be necessary to realize optimal production rates of chemicals[15].

Previous studies have examined the effects of the growth rates of the host organisms and the metabolic stresses inflicted on them, on the proper functioning of the toggle switch[16,17]. There have also been efforts into reducing the burden on host cells caused by the expression of the genetic elements that constitute the toggle switch[14]. A preliminary modeling study has previously indicated the possibility of a trade-off between the speed of switching and bi-stability for symmetric toggle switches in specific parametric ranges[18]. Building on this, we aim to perform a more systematic analysis on the effect of model parameters

on the switching speed and the robustness of the switch over the entire range of feasible parameter values. A formal framework that provides guidelines to engineer better switching behavior in bi-stable motifs would be invaluable in designing circuits for dynamic control applications.

In this work, we first develop a novel dynamical modeling framework to identify the effects of varying the parameters of a bi-stable motif model on its speed of switching and robustness to varying protein production rates, using the genetic toggle switch as a model circuit. We observed that the speed of switching can be improved by increasing the degradation rates of the repressor proteins in the system, similar to previously reported findings on a different genetic circuit [19]. However, this results in a decrease in the range of protein production rates over which the toggle switch remains bi-stable, indicating a trade-off between these two characteristics. Through a systematic analysis of the switching characteristics over a range of biologically relevant parameter values, we identify optimal parameter ranges that result in maximal robustness of the toggle switch. To experimentally validate these findings, we first constructed a representative toggle switch with the repressor proteins coupled to a fluorescent reporter to enable live tracking of the switch's state. We then built a large variant library of our newly developed repressor-reporter fusion toggle switch, to validate the presence of the speed - robustness trade-off that was indicated by our models.

3 Methods

3.1 Mathematical model

The genetic toggle switch was chosen as the model circuit to study the effect of bi-stable motifs. It consists of two repressors that inhibit each others' transcription, resulting in a net positive feedback motif (Figure 1). The state of the switch can be altered by means of external inducers, which act by binding to and inactivating their corresponding repressor targets. The proposed mathematical model for the genetic toggle switch (shown in Eq. 1) was generated using mass action kinetics where $Repressor1$ and $Repressor2$ represent the repressors LacI and TetR in the case of the genetic toggle switch. For the sake of simplicity, we assumed that repressors binding to their cognate promoter targets occurred at a much faster time-scale than the production of the repressor proteins, thereby resulting in an equilibrium between the repressors and their targets. Additionally, we assumed that the rate of transcription and translation can be represented by a lumped parameter (k_p), distinct for each repressor but does not change over the course of the simulation. To simulate the effect of the addition of inducer molecules, the ability of the repressor species to bind to their cognate promoter targets was impacted by increasing the values of the parameter K_{diss} to a very high value, where the repressor could no longer inhibit gene expression from its promoter target.

$$\frac{d[Repressor1]}{dt} = \frac{k_{p1}}{1 + (\frac{[Repressor2]}{K_{diss2}})^{n2}} - k_{deg1} * [Repressor1] \quad \text{(Eq. 1a)}$$

$$\frac{d[Repressor2]}{dt} = \frac{k_{p2}}{1 + (\frac{[Repressor1]}{K_{diss1}})^{n1}} - k_{deg2} * [Repressor2] \quad \text{(Eq. 1b)}$$

where

$[Repressor1], [Repressor2]$: Concentration of repressors (μM)

k_{p1}, k_{p2}: Production rate of repressors ($\mu M/h$)

K_{diss1}, K_{diss2}: Equilibrium dissociation constant for repressors binding to cognate promoters (μM)

n_1, n_2: Cooperativity of repressor binding

k_{deg1}, k_{deg2}: Degradation rate of repressors (h^{-1})

3.2 Dynamical modeling framework

In order to systematically evaluate the effects of perturbing the model parameters on the switch's function, we formulated a general dynamical modeling framework that accepts as its inputs, an ordinary differential equation model of any gene regulatory motif or more generally, dynamical process. Following this, given a set of parameter values, our modeling framework can calculate all the stable and unstable steady states of the model. Further, the framework can also calculate any potential separatrices dividing stable concentration regimes in multi-stable systems by integrating along negative time from an unstable steady state. If the dynamical model possesses multiple stable states, the framework can compute the time that would be required to switch between these states upon the addition of an effector molecule (e.g. IPTG, aTC in the case of the genetic toggle switch). Additionally, we coupled the continuity analysis capabilities of the PyDSTool[20] package in Python to our modeling framework to enable calculation of limit points (parameter values where the behavior of the model changes) and thereby determine stability regimes over parameter ranges for the dynamical system of interest. The framework has been packaged as a Python module will be available on GitHub shortly. It uses functionalities from the scipy[21] and PyDSTool[20] packages of python[21].

3.3 Design and construction of DNA parts and plasmids

The RBS calculator (v2.1) proposed by Reis et al[22] was used to design constructs with varying translation initiation rates(TIRs) or strengths of the Ribosome Binding Sequence (RBS) and to calculate the RBS strengths of previously available constructs, where necessary. The genetic toggle switch constructed by Litcoffsky et al[13] was used as the template to construct the fusion toggle switch, which was then used as the base plasmid for all further constructions. Unique Nucleotide Sequences (UNSs)[23] were added upstream and downstream of each genetic part to improve their modularity and enable rapid assembly of different combinations of genetic parts. Preliminary DNA parts for varying RBS's and protease affinity tags of the repressors were synthesized by Ranomics Inc. Synthetic oligonucleotide parts for DNA assembly reactions were synthesized by Eurofins Scientific and Integrated DNA Technologies Inc. Ligase Cycling Reaction (LCR)[24] and Gibson assembly[25] were used to assemble different DNA parts into complete plasmids. Plasmids were maintained in *E. coli* (DH10β) cells after assembly by transfection through heat shock or electroporation. An Opentrons robotic liquid handler was programmed to perform DNA and plasmid extractions where higher throughput was required. All PCR amplifications for plasmid construction were performed using Q5 High-Fidelity Polymerase (NEB). All plasmids were sequence verified through Sanger sequencing. *E. coli* cells harboring the target plasmids were stored in 20% glycerol at -80°C.

3.4 Characterization of fusion protein constructs and toggle switch variants

The constructed plasmids were transformed into *E. coli* (MG1655) Δ lacI - the target host for final characterization, through electroporation. All strains were characterized using an in-house microplate based high throughput robotic platform that has been previously described[26]. Cells were grown in microtiter plates overnight using LB media supplemented with 1% glucose and the appropriate inducer (2 mM isopropyl β-D-1-thiogalactopyranoside - IPTG or 500 ng/mL anhydrotetracycline - aTc). Following this, they were transferred to fresh Rich Defined Media with the same inducer, supplemented with 1% glucose and allowed to adapt to the new media overnight. Rich defined media (RDM) was used as the growth medium for phenotyping experiments. It is composed of a carbon source (D-glucose at various concentrations), salts (3.5 g/L KH_2PO_4, 5 g/L K_2HPO_4, 3.5 g/L $(NH_4)_2HPO_4$, 1 mM $MgSO_4$, 0.1mM $CaCl_2$), 1 mM 3-morpholinopropane-1-sulfonic acid (MOPS), amino acid supplements (0.8 mM alanine, 5.2 mM arginine, 0.4 mM aspargine, 0.4 mM aspartate, 0.1 mM cysteine, 0.6 mM glutamate, 0.6 mM glutamine, 0.8 mM glycine, 0.2 mM histidine, 0.4 mM isoleucine, 0.8 mM leucine, 0.4 mM lysine, 0.2 mM methionine, 0.4 mM phenylalanine, 0.4 mM proline, 10 mM serine, 0.4 mM threonine, 0.1 mM tryptophan, 0.2 mM tyrosine, and 0.6 mM valine), nucleotide supplements (0.1 mM each of adenine, cytosine, guanine, and uracil), and vitamin supplements (0.01 mM each of thiamine, calcium pantothenate, *p*-aminobenzoic acid, *p*-hydroxybenzoic acid, and 2,3-dihydroxybenzoic acid) - adapted from the defined media composition described previously[27].

To examine the speed of switching, overnight RDM cultures were then washed with RDM media without any inducer to remove traces of the previously used inducer and transferred to fresh rich defined media[27] at a uniform cell density corresponding to OD_{700} of 0.01. The required inducer (2 mM IPTG to strains grown overnight on aTc and 500 ng/mL aTC to strains grown overnight on IPTG) was added to the plates which were then incubated in a Tecan Spark microplate reader at 37°C. The cell densities and concentrations of reporter proteins were monitored by recording absorbance at 700 nm and fluorescence intensities using the following parameters: GFP (Excitation: 488 nm, Emission: 525 nm, Gain: 90), mCherry (Excitation: 570 nm, Emission: 610 nm, Gain: 110). For bi-stability tests, overnight cultures of *E. coli* in RDM containing the appropriate inducer were washed with media lacking inducer to remove all traces of the previously used inducer. Then, cells were inoculated in fresh RDM at a cell density of $OD_{700} = 0.01$ and grown to saturation. Following this, the cells were progressively transferred two more times to fresh media lacking inducer at a 1:100 dilution at 12 hour intervals, with the cell density and fluorescent reporter concentrations being recorded at the end of each transfer.

3.5 Data analysis

Blank subtracted fluorescence values normalized to the measured cell density values were used to track repressor protein levels in the cells. For the switch speed experiments, the time required to switch was calculated as the time taken for the fluorescent reporters to reach their steady state concentrations. This was done by approximating the first derivative of OD normalized fluorescence data and determining the time at which its absolute value becomes lower than a fixed threshold. For bi-stability analysis, the GFP and mCherry fluorescence at the end of each transfer was recorded. The cells were considered stable in their state if the fluorescence values of the corresponding reporter was at a detectable level after each of the three transfers, indicating that the corresponding repressor is also still at high levels. Individual replicates were

considered bi-stable if both states were stable at the end of three transfers and each toggle switch variant strain was considered bi-stable if all the individual replicates were bi-stable after three transfers. Data analyses for all sections were conducted using Python on Jupyter notebooks. The jupyter notebooks used to generate figures and process data in this work, along with a description of each file will be made available on GitHub shortly. The python based data analysis library - pandas and plotting library - plotly were used extensively for all data analysis and visualization pipelines in this work[28,29]. Microbial phenotypic data and growth curves were analyzed using the IMPACT Framework[30].

4 Results & Discussion

4.1 Model description and establishing switch function metrics

The mathematical formulation of the bi-stable architecture that we have proposed tracks the concentration of two repressors and consists of 8 parameters that are engineerable *in vivo*. Specifically, the repressor production rates - k_{p1}, k_{p2} can be altered by modifying the promoter or the ribosome binding sequence to enhance/inhibit transcription and translation rates. The co-operativity of the repressors - n_1, n_2 and their equilibrium dissociation constants - K_{diss1}, K_{diss2} can be altered by modifying the binding sites of the repressors to each other and to their promoter sites. The parameters K_{diss1} and K_{diss2} also signify the concentration of repressors at which their corresponding promoters result in half-maximal production of the other repressor. Finally, the repressor degradation rates - k_{deg1}, k_{deg2} can be increased by adding protease affinity tags to the terminii of the proteins. Among these parameters, the repressor protein production and degradation rates are the easiest to engineer due to the availability of a robust tool to calculate the strength of ribosome binding sites of any DNA sequence[22] and genetic parts that result in varying affinities to proteases[31]. The cooperativity of typically used repressors in synthetic bi-stable motifs - LacI and TetR is 2 and hence, the parameters n_1 and n_2 were set to this value for all our simulations. Additionally, we identified that for bioengineering applications, the speed of switching between the two states and the ability to retain bi-stable behavior in a range of different conditions which may cause variations in protein production rates, are two important characteristics of a desirable bi-stable motif. Hence, we wished to leverage our newly formulated dynamical modeling framework to examine the effects of varying the two engineerable parameters - protein production and degradation rates on these two functional metrics.

Studies have previously shown that protein production rates in cells are highly variable depending on the growth rate, which itself is governed by an array of environmental conditions that cells are exposed to[32,33]. Since our goal is to determine parameter ranges that result in functional bi-stable switches across a range of conditions, we define the robustness of the switch as its ability to retain bi-stable behavior in response variations in protein production rates. Hence, for a given set of other parameter values, we evaluated the values of the repressor production rates k_{p1}, k_{p2} that serve as limit points - points that set the threshold for the motif switching from bi-stable to mono-stable behavior, by performing a two-parameter continuity analysis on the toggle switch model. All parameter values within the region bounded by the motif's limit points will result in a bi-stable configuration, while those outside are mono-stable. As a feasibility limit, we set 1000 µM/h as the maximum possible repressor production rate, which corresponds to the same rate as over 25% of the total cellular protein concentration being produced every hour[34]. We computed the robustness metric as the fraction of the area bounded by the bi-stable region in the protein

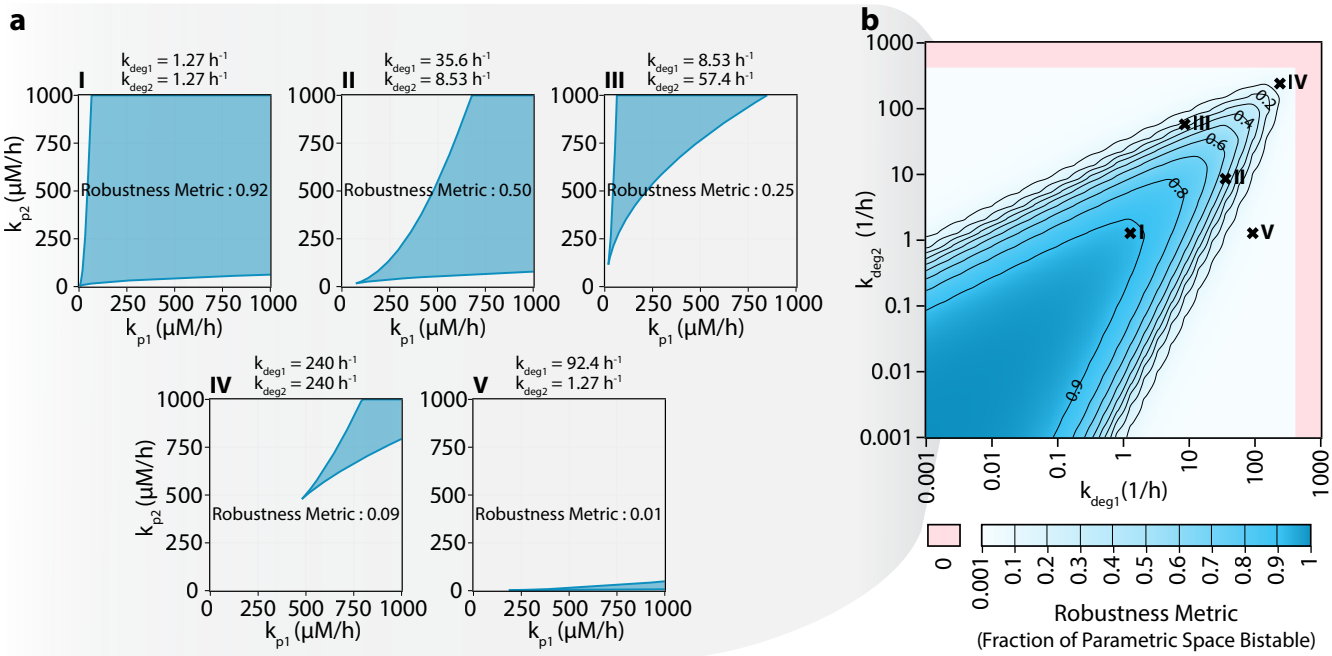

Figure 2: Determination of Robustness Metric: a. Robustness of the bi-stable motif to varying protein production rates. The region of bi-stability for a given set of parameter values can be obtained by performing a two-parameter continuity analysis on a dynamical model of the bi-stable motif. The area bounded within the shaded region corresponds to the range of repressor production rates where the system is bi-stable. The robustness metric is calculated as the fraction of the parametric space that is bi-stable. **b.** Robustness landscape over the entire range of experimentally realizable degradation rates. Continuity analysis on all combinations of feasible degradation rates of the repressor proteins was used to compute the robustness metric for each parameter set.

production parametric space to the entire protein production parametric space (i.e. a robustness metric of 0.1 implies that 10% of all possible protein production rates will result in bi-stable behavior) (Figure 2a).

The speed of switching for a given set of parameters can be characterized by calculating the concentration of the two repressors over time upon the addition of inducers, simulated by altering the DNA binding affinities of the corresponding repressors (K_{diss1}, K_{diss2} set to infinity to simulate the higher affinity of repressors to inducer molecules than their DNA targets)[35]. In our simulations, the speed of switching was determined as the multiplicative inverse of the time taken for either repressor to reach 99.99% of their steady state concentrations Figure 3c, d. While the robustness metric directly incorporates all feasible production rates (k_{p1} and k_{p2}) into its calculation, the speed metric does not, and may vary within the parameter bounds set by our robustness calculations. Hence, we calculated the speed metric as the inverse of the average time taken to switch between the states using repressor production rates at the four extrema of the robustness metric curve (Figure 3). We observed that our speed metric is largely intransigent to variations in the repressor production rates, with deviations from the mean value limited to less than 5% for most cases analyzed (Figure S1).

4.2 Speed-robustness trade-off emerges in the toggle switch model

Having established standard metrics to evaluate the switch's function for a given parameter set, we wished to perform a preliminary analysis of our bi-stable motif's functioning for a test case where the equilibrium

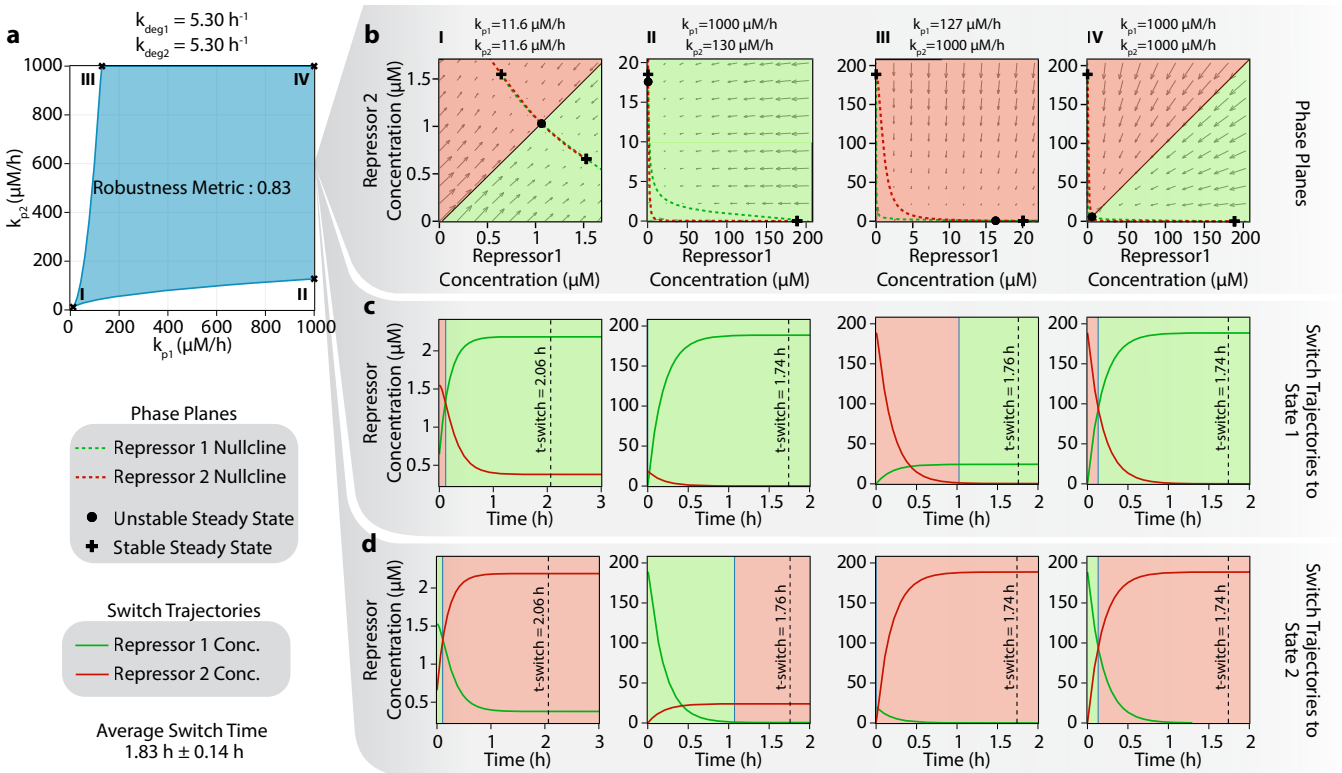

Figure 3: Determination of Speed Metric: a. Parameter values from the extrema of the robustness analysis are used to perform a simulation of the ordinary differential equations describing the bi-stable motifs and obtain **b.** the phase plane and **c., d.** the switch trajectories to either state using our dynamical modeling framework. The average time taken to switch to either state is first determined and the switch speed is calculated as the multiplicative inverse of the average switch time.

dissociation constants K_{diss} for both repressors was set to 1 μM. This parameter value is consistent with *in vivo* observations made in previous studies for the Lac repressor and corresponds to roughly 600 copies of the repressor protein resulting in half-maximal repression of the cognate promoter in a single *E. coli* cell[36]. We computed robustness values for combinations of degradation rates of the repressor proteins spanning 6 orders of magnitude - ranging from 0.001 h^{-1} to 1000 h^{-1} (as feasibility thresholds for protein degradation rates, corresponding to a protein half-life of 693 hours and 2.5 seconds respectively) (Figure 2b). Robustness values showed a decreasing trend with increasing degradation rates, with infeasible regions (where no bi-stable configuration was possible), at very high degradation rates (repressor half life <4 seconds). Additionally, for each value of the protein degradation rate, maximum robustness was observed when both repressors had the same degradation rate, with robustness values dropping drastically with imbalances in these rates.

We observed that imbalances in the degradation rates of the repressors also resulted in impaired switching speeds (Figure 4a). However, in contrast to the trends observed for robustness, the speed of switching showed an increase (corresponding to a decrease in the time required to switch) with increasing degradation rates, reaching a maximum at the highest feasible combination of degradation rates. These results indicate that while switches can be made faster through the addition of protease affinity tags, there is a trade-off between the speed and robustness of the switch. Also, there is a maximum threshold on the speed of switching, which is determined by the maximal feasible value of the degradation rates, as determined from

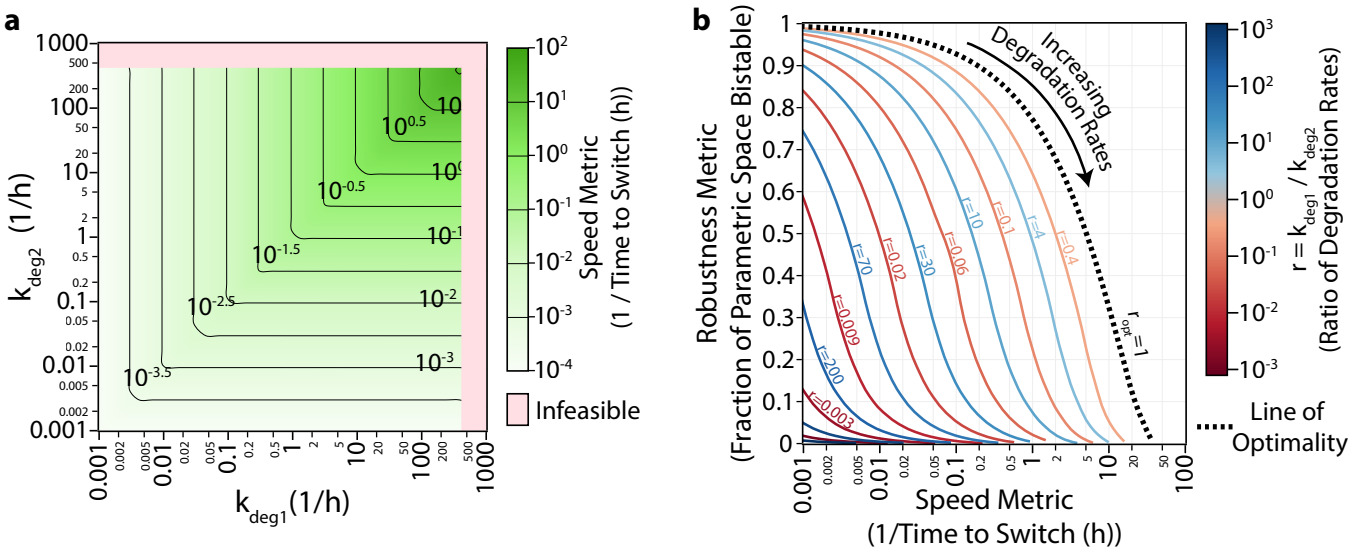

Figure 4: a. Speed metric landscape over the entire range of feasible repressor degradation rates for K_{diss}=1 for both repressors. **b.** Speed metric vs. Robustness metric for each ratio of repressor degradation rates with K_{diss}=1.

the robustness calculations.

In order to better understand the relationship between the two switch metrics, we plotted the robustness and speed metric values arising from all of our parameter sets (Figure 4b). We observed that for any given ratio of degradation rates (denoted 'r') of the two repressors, the speed and robustness metrics show a clear trade-off - as the speed metric increases, the robustness metric drops which can be realized by moving along the lines depicted in Figure 4b. Interestingly, there is an optimal value of 'r' that forms an upper bound for the maximal robustness for any given switching speed and this value for our preliminary parameter set is 1 - where, the degradation rates of the two repressors are equal.

Following this, we wished to examine the trends in robustness and switch speeds over the entire range of feasible parameter values. Keeping the co-operativity constant at 2, we varied the equilibrium dissociation constants of the repressors over 5 orders of magnitude ranging from 0.005 µM to 500 M (corresponding to 3 copies and 300,000 copies of the repressor protein respectively in each cell, assuming the same volume as *E. coli*). This upper bound on the K_{diss} values represents approximately 10% of the cell's entire protein budget[34]. We find that the robustness landscapes across all parameter sets show the same decreasing trend with increasing protein production rates as observed in our preliminary parameter set (Figure 5). However, in contrast to our preliminary parameter set, we found that the robustness and consequently, the range of feasible degradation rates and becomes smaller with increasing K_{diss} (which represents impaired repression by the repressor). These results indicate that a bi-stable motif that employs repressors with enhanced DNA binding capabilities will perform better than those that use weakly binding repressors. While the robustness metric showed significant differences with changing K_{diss} values, the speed metric remained constant over the entire range of K_{diss} values, with only the feasibility region becoming smaller with poorer repressor-DNA binding (Figure S2). Along with our previous observation that the switch speed does not change with repressor production rates, this result indicates that the only parameter in our model that affects the switch speed significantly is the degradation rate of the repressor proteins.

Interestingly, upon analyzing the speed-robustness relationship for all combinations of K_{diss} values,

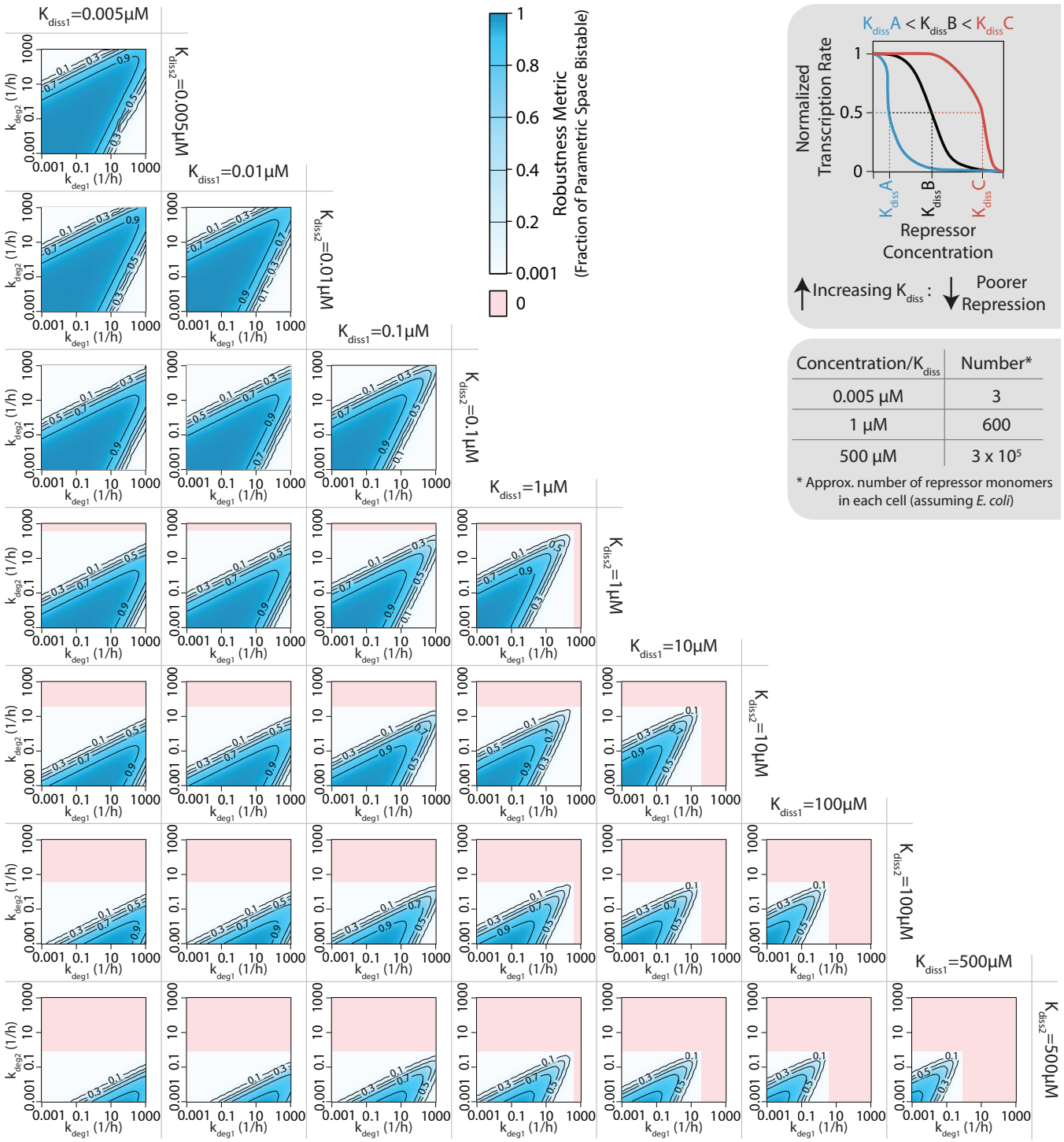

Figure 5: Robustness landscape for all feasible parameter combinations. The robustness landscape over all feasible protein degradation rates, calculated for different combinations of K_{diss} values that represent the physical limits of experimentally observable values for the parameter. The shaded boxes to the top-right illustrate the physical significance of the parameter - K_{diss}.

we observed that the optimal ratio of degradation rates (r_{opt}) that resulted in maximum robustness at a given speed metric, changed with different combinations of K_{diss} values (Figure 6). Specifically, when the values of the dissociation constants for the two repressors remained equal, the r_{opt} remained equal to

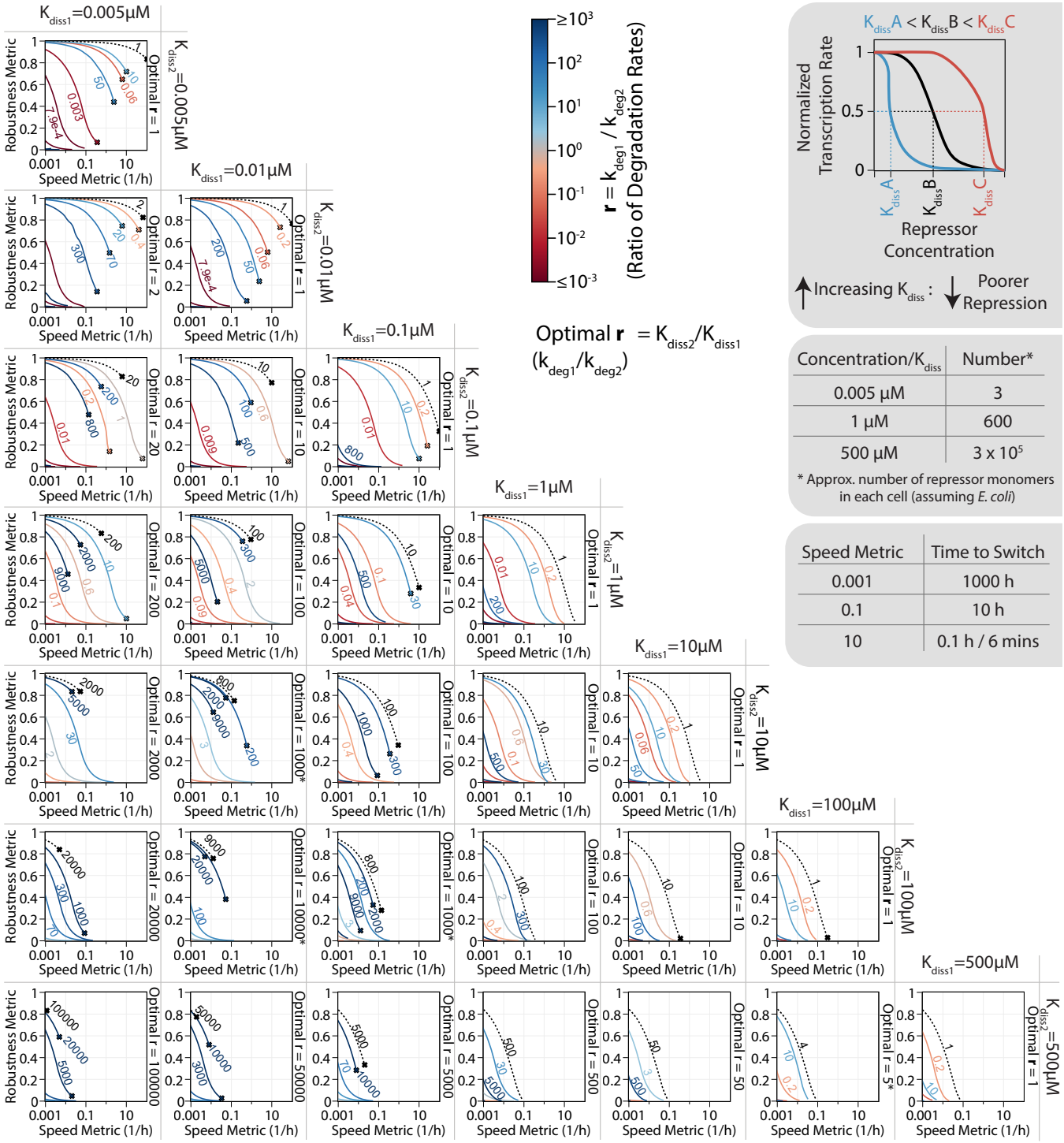

Concentration/K_{diss}	Number*
0.005 μM	3
1 μM	600
500 μM	3×10^5

* Approx. number of repressor monomers in each cell (assuming *E. coli*)

Speed Metric	Time to Switch
0.001	1000 h
0.1	10 h
10	0.1 h / 6 mins

Figure 6: Relationship between the speed metric and robustness metric over entire feasible parametric range. The relationship between the speed and robustness metrics plotted for all combinations of K_{diss} values that represent the physical limits of experimentally observable values for the parameter. The shaded boxes to the top-right illustrate the physical significance of the parameter - K_{diss}.

1. As the dissociation constants of the two repressors change, the r_{opt} changes correspondingly, seemingly trying to balance out the imbalance caused by different binding affinities of the two repressors to their cognate promoter targets. This finding is very important while designing bi-stable motifs with two different

repressors as in the case of the genetic toggle switch, in order to determine the optimal protease tag to add to each repressor.

4.3 Repressor-reporter fusion to characterize switch state in real time

Following the discovery of design guidelines to build better bi-stable motifs, we wished to validate our model findings by building faster switching variants of the genetic toggle switch described by Litcofsky et al[13]. Additionally, we also wanted to demonstrate the presence of a speed-robustness trade-off experimentally. In order to monitor the speed of switching, it is necessary to track the concentrations of the repressor proteins *in vivo* to determine when a state change has occurred. However, in the original design of the toggle switch, the repressor and fluorescent reporter proteins are de-coupled, precluding a quantitative analysis of repressor concentrations by simply measuring the fluorescence intensities of the reporters. Hence, we aimed to construct a fusion variant of the genetic toggle switch where the repressor and reporter proteins are physically coupled to each other by means of the flexible protein linker - $(GGGGS)_2$[37]. In order to determine the optimal configuration of the repressor-reporter fusions (N-terminal vs C-terminal fusions) that resulted in similar repression characteristics as their non-fusion counterparts, we constructed all possible variants of fusion constructs of the LacI repressor with the fluorescent protein GFP, and the TetR repressor with the fluorescent protein mCherry. We then inserted these constructs into test circuits where they would control expression of a fluorescent protein and can be induced with their cognate inducer (IPTG for LacI and aTc for TetR). The test circuits used for each repressor, shown in Figure 8 consist of GFP or mCherry under the control of either the p_L or $pTrc$ promoter respectively. The fusion constructs with TetR or LacI were expressed constitutively as required in the test plasmid constructs, repressing production of the fluorescent reporters GFP and mCherry, until they are sequestered through the addition of aTC or IPTG respectively..

In our designs, we observed that neither configuration for both repressors resulted in a significant increase in leaky expression (expression of downstream genes without the addition of inducers) from their target promoters, indicating that the fusion constructs are at least as good as their wild-type counterparts in DNA binding ability (Figure S3). Additionally, we also examined the ability of the repressors to be induced by their corresponding inducer molecules. In all cases, the fusion constructs showed weaker induction characteristics than their wild-type counterparts, with higher concentrations of inducer being required for an equivalent de-repression of their promoters. We chose the fusion protein configuration that had a lower K_M (inducer concentration required for half maximal expression) and lower variance in induction characteristics. Hence, the TetR-mCherry (TetR at N-terminus and mCherry at C-terminus) and GFP-LacI(GFP at N-terminus and LacI at C-terminus) fusion proteins were chosen as optimal constructs for further experiments.

4.4 Constructing and characterizing a diverse toggle switch library

Having determined the optimal configuration of fusion proteins to ensure that the DNA binding and inducer binding abilities of repressor proteins are minimally affected, we assembled our representative toggle switch using GFP-LacI and TetR-mCherry as the repressors, with the ribosome binding strength of either repressor engineered to mimic the values found in the original pKDL071 version of the toggle switch[13] (shown in Table S1). Our fusion toggle switch functioned as expected, displaying high mCherry fluorescence

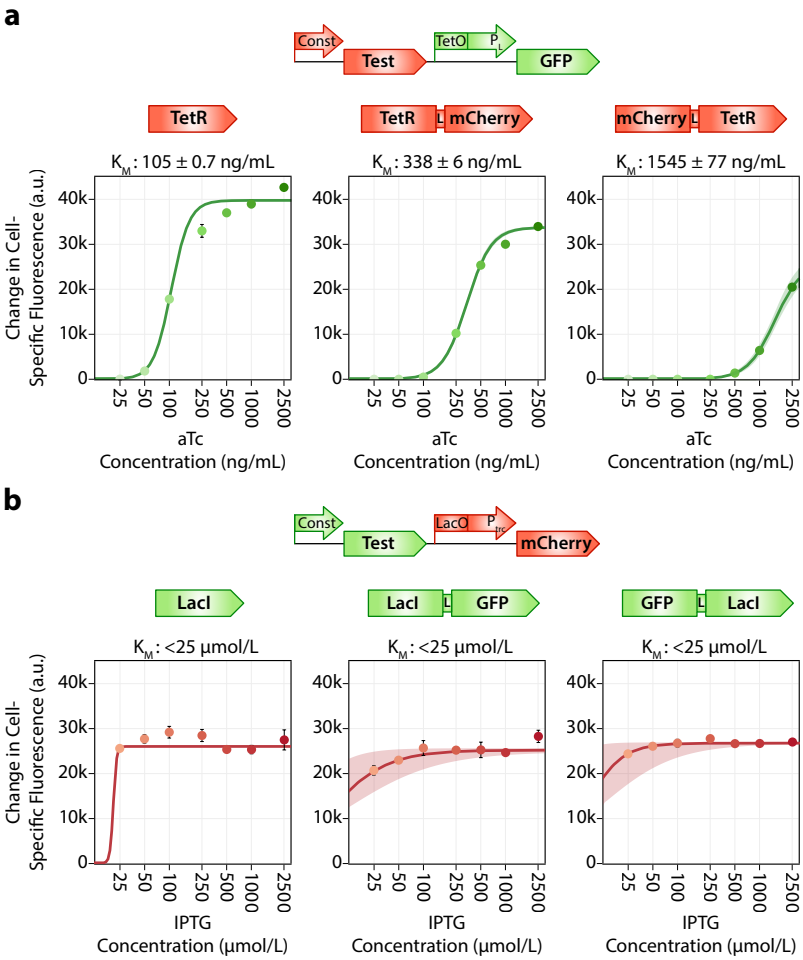

Figure 7: Test Circuits and Results for Fusion Protein Characterization. The test circuits to examine the induction of **a.** TetR and **b.** LacI fusion proteins are shown with the corresponding induction profiles for each of the fusion protein variants. 'L' refers to the protein linker used to build the repressor-reporter fusions. For each case, the difference in cell-specific fluorescence between cells induced with various inducer concentrations and uninduced cells is shown. A Hill kinetics equation was fit to this data to obtain the Michaelis-Menten constant K_M.

(and correspondingly high TetR concentrations) when grown on IPTG and high GFP fluorescence (and correspondingly high LacI concentrations) when grown on aTc (Figure S4). However, the construct seemed to have lost bi-stability, reverting to a TetR high state after the removal of aTc, resulting in mono-stable constructs. This is possibly due to variations in the protein production rates effected by the calculated RBS values resulting in imbalances in the switch. Nevertheless, we used this construct as starting point to construct our variant library, since we would be able to restore bi-stability by altering the RBS strengths if our model predictions are accurate.

Next, we designed variants of the fusion toggle switch with varying ribosome binding site(RBS) strengths and protease affinity tags to create constructs that result in a range of protein production and degradation rates, as required to validate our model findings. To this end, we designed RBSs that we expected to show between 2 and 30 times the strength of the RBS in the original toggle switch - pKDL071 using the RBS calculator (v2.1)[22] (Table S1). In order to vary the degradation rates of the toggle switch proteins, we leveraged the native *ClpXP* protease in *E. coli* by tagging the repressors with the SsrA tag and its variants

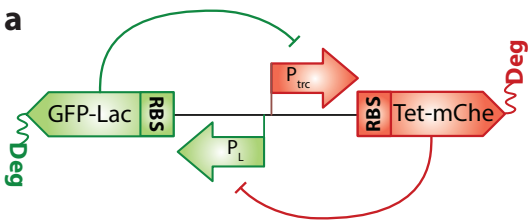

b RBS

RBS Name	Strength (TIR)
A	~ 2x pKDL071*
B	~ 5x pKDL071*
C	~ 10x pKDL071*
D	~ 20x pKDL071*
E	~ 30x pKDL071*

*pKDL071 refers to the strength of the RBS in the original toggle switch - pKDL071

c Deg

Tag Name	Tag AA Sequence
No Tag	*
DAS	AANDENY--A**DAS***
DAS+2	AANDENY**NY**A**DAS***
LAA	AANDENY--A**LAA***

*Stop codon

Figure 8: Fusion Toggle Switch Architecture to Study Speed-Robustness Trade-off. a. An illustration of the fusion toggle switch with GFP-LacI and TetR-mCherry with modified ribosome binding site (RBS) and added degradation tags. **b.** The five RBS strengths (as predicted by RBS calculator v2.1[22]) chosen for each repressor relative to its value on the original pKDL071 toggle switch designed by Litcofsky et al[13]. The queries and translation rates corresponding to each RBS level is shown in Table S1. **c.** Degradation tags and their amino acid sequences added to the repressors for toggle switch library construction. Modified versions of the SsrA degradation tag that show different degradation rates were chosen.

that have been used in previous studies to show graded degradation rates[31,38]. A list of RBS strengths and degradation tags we chose for each repressor are shown in Figure 8. This resulted in 20 variants of each fusion repressor, composed of all possible combinations of the RBSs and degradation tags.

To shortlist functioning RBS and degradation tags for our final combinatorial library, we first examined the protein production and degradation rates of the 20 variants of each fusion repressor leaving the other repressor unchanged (40 constructs in total), by transforming plasmids harboring these constructs into *E. coli* MG1655 (ΔlacI) and inducing their expression with IPTG or aTc. We then monitored the levels of repressor proteins produced by the RBS-degradation tag combinations by recording the fluorescence intensity of the reporter attached to them. As expected, the addition of degradation tags resulted in progressively higher rates of degradation of the repressors and consequently, lower steady state fluorescence intensities from the reporter attached to them (Figure 9b, d). Furthermore, the strengths of the degradation tags indicated by these results are largely in line with observations made in previous studies ('LAA' has the highest strength, followed by 'DAS+2' and then 'DAS')[38]. The relative rates of degradation, as indicated by the reduction in the steady-state fluorescence intensity at each RBS level were estimated and have been listed in Table S2 and Table S3.

However, RBS strengths did not conform with our design parameters, specifically for TetR-mCherry, with many RBSs constructs showing minimal variation (Figure 9a, c). Hence, we shortlisted 10 combinations of RBS-degradation tag variants for each repressor, that showed the largest variability in the fluorescence intensities (and consequently the repressor production/degradation rates) in order to obtain a highly variable combinatorial library of toggle switch variants and thereby examine a large portion of the design space. We then constructed plasmids containing all possible combinations of the variants using the ligase cycling reaction method[24], sequence confirmed the 100 resulting plasmids, and transformed them into *E. coli* MG1655 (ΔlacI) for final characterization.

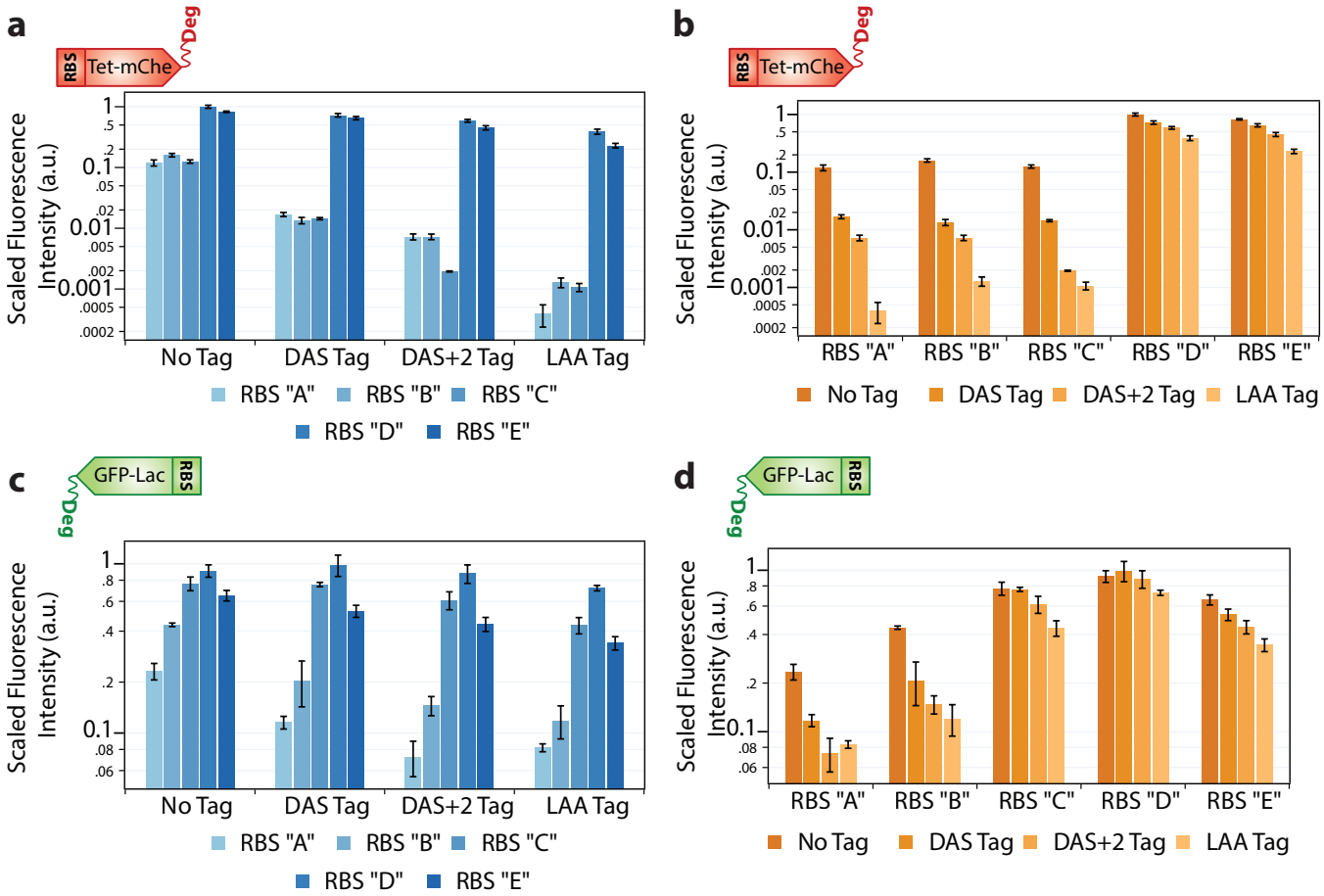

Figure 9: Characterization of RBS and degradation tag variants of fusion repressor proteins. Fluorescence intensities of the repressor-reporter fusion constructs determined for each of the 20 RBS-degradation combinatorial variants for **a.** TetR-mCherry separated by the degradation tag used, **b.** TetR-mCherry separated by the RBS used **c.**GFP-LacI separated by the degradation tag used, **d.** GFP-LacI separated by the RBS used.

4.5 Switch variants show a wide range of switching speeds

Leveraging the previously described high-throughput phenotyping platform [26], we examined the switching speed of our 100 switch variants in triplicate. We monitored the time taken by either repressor to reach its steady state maximum and minimum upon the addition of the corresponding inducer (Figure 10a). As expected, adding degradation tags and thereby increasing the degradation rates of the Tet repressor resulted in a generally faster rate of the Tet repressor reaching its steady state value in both states. In particular, the addition of degradation tags greatly reduced the time taken to degrade TetR from cells that are switching into the Lac high state, as indicated by the large reduction in the Tet degradation time for our library variants compared to the original construct (Figure 10b). We observed a similar trend with the Lac repressor as well, with many library variants with degradation tags showing a shorter time to reach the steady state value (Figure 10c). There were however, some Lac repressors with relatively low degradation rates (as predicted in Table S2 and Table S3) that reached steady state much faster than those with higher degradation rates, possibly due to their extremely low RBS levels, resulting in very small steady state values.

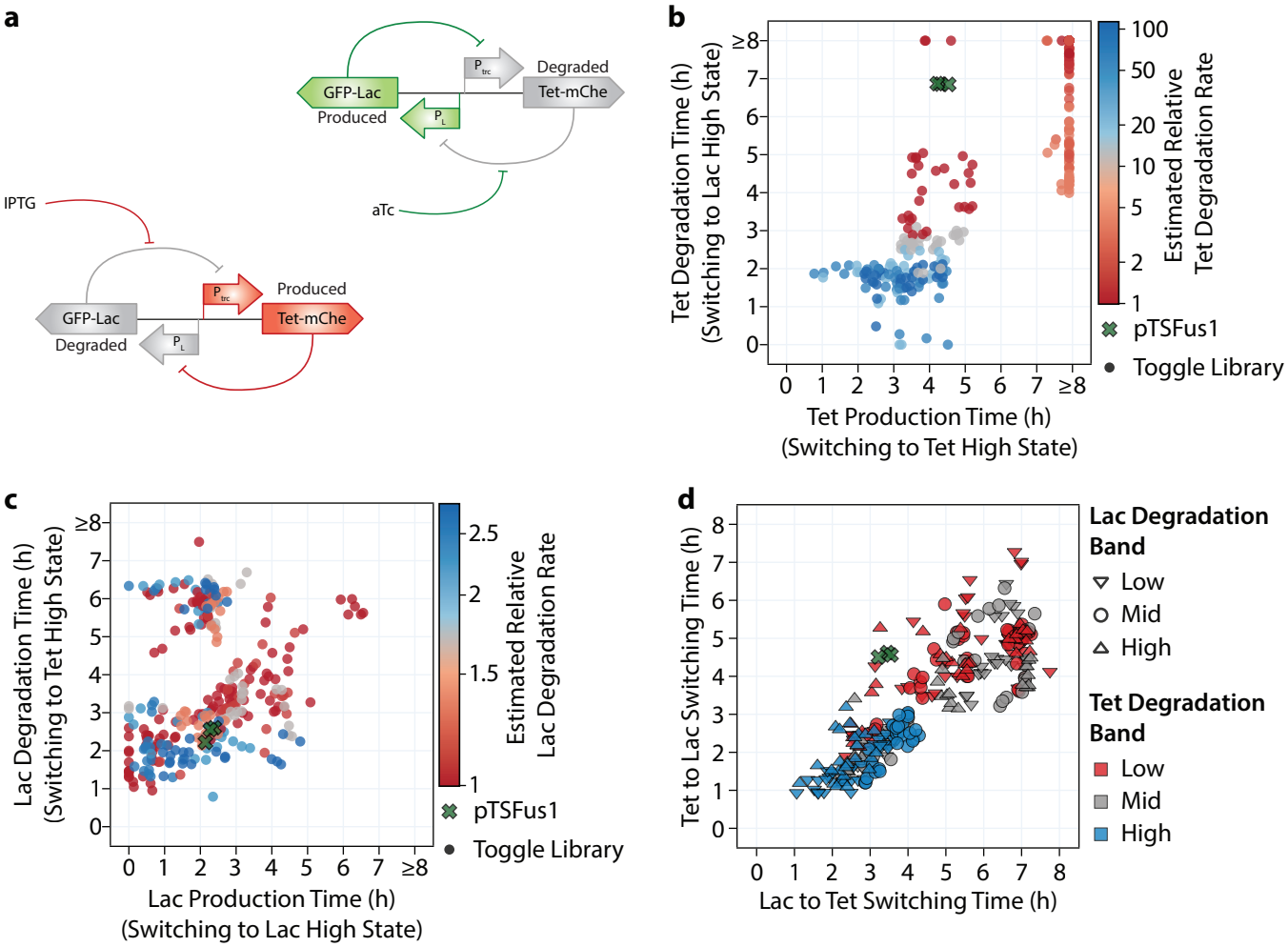

Figure 10: Switching time vs Degradation rates. **a.** Illustration showing the addition of different inducers and which repressors are produced or degraded in each case. The time taken by either repressor to be produced and degraded in the appropriate state is calculated. **b.** Effect of degradation tags on the Tet repressor in reaching steady state concentrations. **c.** Effect of degradation tags on the Lac repressor in reaching steady state concentrations. **d.** Effect of degradation tags on the switching time(calculated as the average of the time taken to produce and degrade the appropriate repressor for each state), with strains classified based on degradation levels estimated in Table S2 and Table S3

Nevertheless, upon comparing the effect of various degradation rates on the overall switching time (mean value of the time taken to degrade one repressor and produce another), we found that those constructs with higher degradation rates, generally resulted in faster switching to either state (Figure 10d) as predicted by our model. Specifically, we found that the degradation tags on the Tet repressor are highly effective in mediating a faster switch, likely due to the higher relative degradation rates in the Tet repressor than the Lac repressor. However, in contrast to our model predictions, several constructs with intermediate degradation rates resulted in very slow switching. Upon a closer analysis, we found that these were constructs with extremely high protein production rates, which resulted in very slow growth and consequently, slower switching than even those constructs without degradation tags. This can be clearly seen when the switching times are plotted against the growth rates of the corresponding cells, where a number of variants with intermediate degradation rates result in very slow growth and therefore slow switching (Figure S5).

A principal component analysis performed on these metrics also confirmed this observation, showing a strong negative correlation between the switching time and growth rate for either state(Figure S6b). Consequently, constructs with intermediate degradation rates resulted in slow switching only when the growth rate was low (Figure S6a). Hence, the growth rate of the resultant strains is an important parameter that also needs to be considered while designing switches. Regardless, our variant library consists of switches that show a wide range of switching time, many of which are faster than the initial construct, indicating that varying the degradation rates is indeed an effective strategy to alter switching speeds. Furthermore, we generally observed that higher degradation rates result in faster switching when the growth rate is constant (Figure S5 and Figure S6).

4.6 Trade-offs in switch function - experimental validation

Having confirmed the effect of adding degradation tags on the speed of switching, we examined the ability of our switch variants to retain their state after removal of their corresponding inducer i.e. the ability to maintain high levels of Tet after IPTG is removed and maintain high levels of Lac after aTc is removed. Based on their ability to retain their state after three consecutive transfers with no inducer, we classified the individual experimental replicates as - Bi-stable when both states are stable, Mono-stable when only either one of the Tet or Lac state is stable and unstable when the construct is unable to retain either state (Figure 11a). Our results show that a majority of strains with low degradation rates are bi-stable, with the proportion of bi-stable strains decreasing as degradation rates are increased. We find the lowest proportion of bi-stable strains in the constructs with the highest degradation rates on both repressors. This is in remarkable agreement with our model findings where robustness (i.e. the region of bi-stability and consequently the number of bi-stable constructs) decreased with increasing degradation rates. Additionally, we also found that increasing the degradation rate of one repressor resulted in more constructs becoming mono-stable towards the other. Additionally, imbalanced degradation rates also resulted in lower robustness, as predicted by our model. We observed the same trends when the experimental replicates of each strain were combined to obtain the overall bi-stability of a construct as opposed to the individual replicates (Figure S7).

Next, we compared the number of bi-stable strains at each level of switching speed to study any possible correlations between the robustness and the speed metric. Once again, in remarkable agreement with our model predictions, we found a monotonically decreasing trend in the proportion of bi-stable constructs, with increasing switching speeds (or decreasing switching times) (Figure 11b and Figure S8). This confirms the presence of a trade-off between the switching speed and robustness in the genetic toggle switch, indicating the need to carefully design switches with appropriate protein production and degradation rates. Importantly, we identify a range of different switch constructs that are fast switching while still being bi-stable. Additionally, since we uncovered previously that the growth rate of the host varies significantly depending on the switch configuration and fast growth is a highly desirable characteristic in metabolic engineering applications, we wished to identify optimally performing switch constructs that switch fast and remain bi-stable, while not imparting a severe growth burden on the host. Comparing the switching time, growth rate and the bi-stability of each strain, we found that all replicates of the construct with the 'E-LAA' Lac repressor and the 'C-DAS+2' Tet repressor resulted in optimal characteristics and can be investigated for further improvement (Figure 11c and Figure S9).

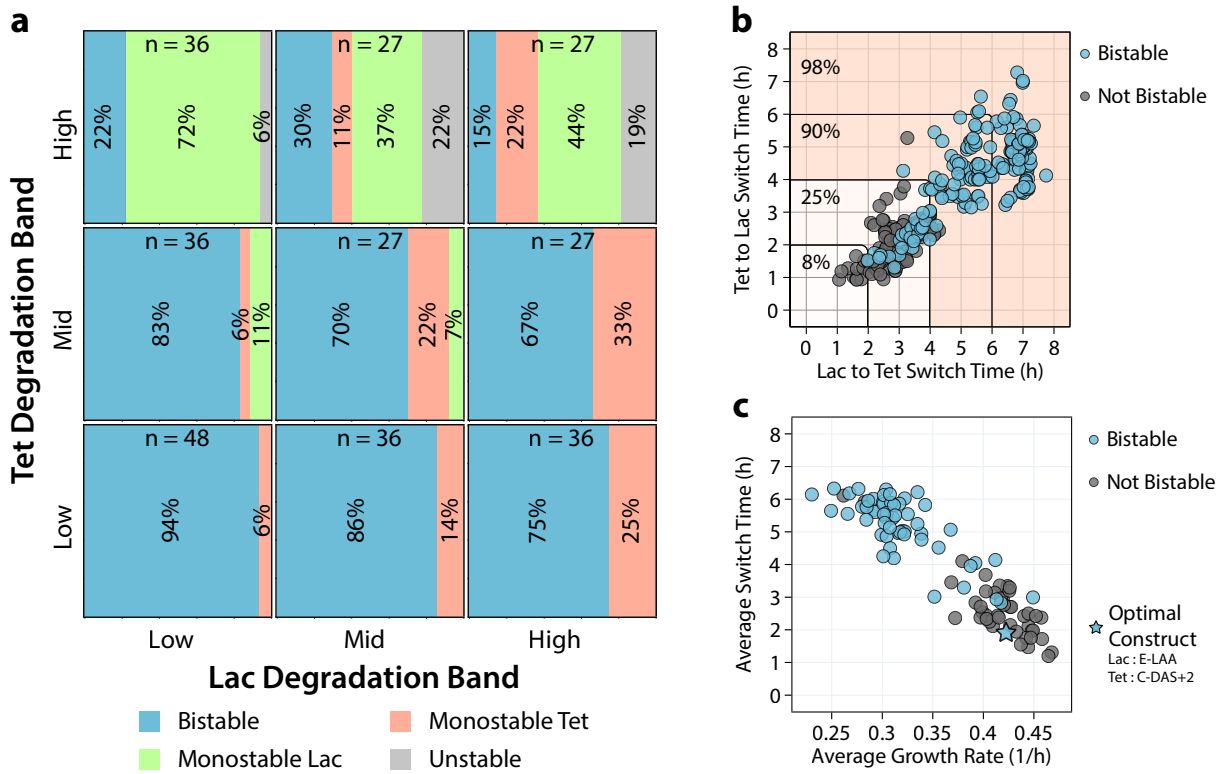

Figure 11: Trade-offs in toggle switch behavior: a Effect of varying degradation levels of the Lac and Tet repressor on the bi-stability of individual replicates. The percent of bi-stable, mono-stable and unstable constructs are shown within the boxes representing each degradation level combination. Constructs were classified into different degradation levels as shown in Table S2 and Table S3. Overall data for each construct is shown in Figure S7. **b.** The Lac state and Tet state switching times for individual replicates, classified based on stability. The percent of bi-stable replicates at each level of Tet and Lac switching times is shown within the plot. Overall data for each construct is shown in Figure S8. **c.** A trade-off between the average switching time (calculated as the average of the two state-switching times) and the growth rate of the each strain, classified based on stability. Constructs were designated bi-stable if all individual replicates were bi-stable. Individual replicate data shown in Figure S9.

5 Conclusions

We have seen here that the design choices made during the construction of bi-stable motifs impacts their function to a great extent. Using a simple mass-action kinetics based model of the toggle switch, we have established a fundamental trade-off between the speed and robustness of bi-stable motifs. Additionally, we have also uncovered ways to engineer the toggle switch to accelerate the switching between the states. Further, we also showed that the growth rate of cells is highly influential in determining the characteristics of switching and is in turn influenced by the production and degradation rates of the switch proteins. These findings could be influential in designing bi-stable motifs for metabolic engineering and therapeutic applications. Moreover, our generalized dynamical model analysis framework could be used to analyze other regulatory motifs and could be a very useful tool in designing complex biological circuits.

Further, we evaluated the presence of the speed-robustness trade-off by constructing a fusion variant of the toggle switch that accurately tracks repressor concentrations. This toggle switch could serve as an invaluable tool in dynamic control applications since the state of the switch can be readily determined by simply monitoring the fluorescence of the cells, in a non-invasive manner. Interestingly, we observed that in our experiments, there were several constructs in the highest Tet degradation band that were not bi-stable or mono-stable in either state (Figure 11a). This deviates from our predictions since based on our deterministic model, toggle switch constructs can be either bi-stable or mono-stable in one state. Stochastic effects where a change in switch state effected by noise in the system could explain this and should be considered in future modeling efforts. Furthermore, the effects of the growth rate of host cells on circuit function and vice versa should be explored further by using models of cellular resource allocation to predict growth rates when heterologous proteins are expressed in host cells. One potential way to alleviate the burden of expressing the toggle switch proteins is to build a variant library in a single copy vector or through genomic integration of the circuit as shown in a recent study[14]. Regardless, our combinatorial library of toggle switch variants show a wide range of switching speeds while remaining bi-stable and could be used to enhance the production of a diverse range of target compounds by decoupling growth and production phenotypes. We anticipate that this work will encourage the widespread use of bi-stable motifs in bioengineering for dynamic control of metabolism.

Acknowledgements

This work was supported by the Natural Sciences and Engineering Research Council (NSERC), the NSERC Industrial Biocatalysis Network, the Ontario Ministry of Research and Innovation, and Genome Canada.

References

[1] Timo Hardiman, Karin Lemuth, Markus A. Keller, Matthias Reuss, and Martin Siemann-Herzberg. Topology of the global regulatory network of carbon limitation in Escherichia coli. *J. Biotechnol.*, 132(4):359–374, 2007.

[2] Joe Lutkenhaus. The regulation of bacterial cell division: A time and place for it. *Curr. Opin. Microbiol.*, 1(2):210–215, 1998.

[3] Andrea Pitzschke, Adam Schikora, and Heribert Hirt. MAPK cascade signalling networks in plant defence. *Curr. Opin. Plant Biol.*, 12(4):421–426, 2009.

[4] Uri Alon. Network motifs: Theory and experimental approaches. *Nat. Rev. Genet.*, 8(6):450–461, 2007.

[5] James E. Ferrell. Feedback regulation of opposing enzymes generates robust, all-or-none bistable responses. *Curr. Biol.*, 18(6):R244–R245, 2008.

[6] Timothy S. Gardner, Charles R. Cantor, and James J. Collins. Construction of a genetic toggle switch in Escherichia coli. *Nature*, 403(6767):339–342, 2000.

[7] Naveen Venayak, Kaushik Raj, Rohil Jaydeep, and Radhakrishnan Mahadevan. An Optimized Bistable Metabolic Switch to Decouple Phenotypic States during Anaerobic Fermentation. *ACS Synth. Biol.*, 7(12):2854–2866, oct 2018.

[8] William Bothfeld, Grace Kapov, and Keith E.J. Tyo. A Glucose-Sensing Toggle Switch for Autonomous, High Productivity Genetic Control. *ACS Synth. Biol.*, 6(7):1296–1304, jul 2017.

[9] David T. Riglar, Tobias W. Giessen, Michael Baym, S. Jordan Kerns, Matthew J. Niederhuber, Roderick T. Bronson, Jonathan W. Kotula, Georg K. Gerber, Jeffrey C. Way, and Pamela A. Silver. Engineered bacteria can function in the mammalian gut long-term as live diagnostics of inflammation. *Nat. Biotechnol.*, 35(7):653–658, may 2017.

[10] Jonathan W. Kotula, S. Jordan Kerns, Lev A. Shaket, Layla Siraj, James J. Collins, Jeffrey C. Way, and Pamela A. Silver. Programmable bacteria detect and record an environmental signal in the mammalian gut. *Proc. Natl. Acad. Sci. U. S. A.*, 111(13):4838–4843, 2014.

[11] Clement T.Y. Chan, Jeong Wook Lee, D. Ewen Cameron, Caleb J. Bashor, and James J. Collins. 'Deadman' and 'Passcode' microbial kill switches for bacterial containment. *Nat. Chem. Biol.*, 12(2):82–86, feb 2016.

[12] Finn Stirling, Lisa Bitzan, Samuel O'Keefe, Elizabeth Redfield, John W.K. Oliver, Jeffrey Way, and Pamela A. Silver. Rational Design of Evolutionarily Stable Microbial Kill Switches. *Mol. Cell*, 68(4):686–697.e3, nov 2017.

[13] Kevin D. Litcofsky, Raffi B. Afeyan, Russell J. Krom, Ahmad S. Khalil, and James J. Collins. Iterative plug-and-play methodology for constructing and modifying synthetic gene networks. *Nat. Methods*, 9(11):1077–1080, nov 2012.

[14] Jeong Wook Lee, Andras Gyorgy, D. Ewen Cameron, Nora Pyenson, Kyeong Rok Choi, Jeffrey C. Way, Pamela A. Silver, Domitilla Del Vecchio, and James J. Collins. Creating Single-Copy Genetic Circuits. *Mol. Cell*, 63(2):329–336, jul 2016.

[15] Kaushik Raj, Naveen Venayak, and Radhakrishnan Mahadevan. Novel two-stage processes for optimal chemical production in microbes. *Metab. Eng.*, 62:186–197, nov 2020.

[16] Jordan J. Sickle, Congjian Ni, Daniel Shen, Zewei Wang, Matthew Jin, and Ting Lu. Integrative Circuit-Host Modeling of a Genetic Switch in Varying Environments. *Sci. Rep.*, 10(1):1–9, may 2020.

[17] Rong Zhang, Jiao Li, Juan Melendez-Alvarez, Xingwen Chen, Patrick Sochor, Hanah Goetz, Qi Zhang, Tian Ding, Xiao Wang, and Xiao Jun Tian. Topology-dependent interference of synthetic gene circuit function by growth feedback. *Nat. Chem. Biol.*, 16(6):695–701, apr 2020.

[18] Jiunn R. Chen. Improving the speed of the genetic toggle switch without sacrificing its dynamic stability. *Phys. Rev. E - Stat. Nonlinear, Soft Matter Phys.*, 73(4):041901, apr 2006.

[19] Daniel Huang, William J. Holtz, and Michel M. Maharbiz. A genetic bistable switch utilizing nonlinear protein degradation. *J. Biol. Eng.*, 6(1):9, 2012.

[20] Robert Clewley. Hybrid models and biological model reduction with pydstool. *PLOS Computational Biology*, 8(8):1–8, 08 2012.

[21] Pauli Virtanen, Ralf Gommers, Travis E. Oliphant, Matt Haberland, Tyler Reddy, David Cournapeau, Evgeni Burovski, Pearu Peterson, Warren Weckesser, Jonathan Bright, Stéfan J. van der Walt, Matthew Brett, Joshua Wilson, K. Jarrod Millman, Nikolay Mayorov, Andrew R.J. Nelson, Eric Jones, Robert Kern, Eric Larson, C. J. Carey, İlhan Polat, Yu Feng, Eric W. Moore, Jake VanderPlas, Denis Laxalde, Josef Perktold, Robert Cimrman, Ian Henriksen, E. A. Quintero, Charles R. Harris, Anne M. Archibald, Antônio H. Ribeiro, Fabian Pedregosa, Paul van Mulbregt, Aditya Vijaykumar, Alessandro Pietro Bardelli, Alex Rothberg, Andreas Hilboll, Andreas Kloeckner, Anthony Scopatz, Antony Lee, Ariel Rokem, C. Nathan Woods, Chad Fulton, Charles Masson, Christian Häggström, Clark Fitzgerald, David A. Nicholson, David R. Hagen, Dmitrii V. Pasechnik, Emanuele Olivetti, Eric Martin, Eric Wieser, Fabrice Silva, Felix Lenders, Florian Wilhelm, G. Young, Gavin A. Price, Gert Ludwig Ingold, Gregory E. Allen, Gregory R. Lee, Hervé Audren, Irvin Probst, Jörg P. Dietrich, Jacob Silterra, James T. Webber, Janko Slavič, Joel Nothman, Johannes Buchner, Johannes Kulick, Johannes L. Schönberger, José Vinícius de Miranda Cardoso, Joscha Reimer, Joseph Harrington, Juan Luis Cano Rodríguez, Juan Nunez-Iglesias, Justin Kuczynski, Kevin Tritz, Martin Thoma, Matthew Newville, Matthias Kümmerer, Maximilian Bolingbroke, Michael Tartre, Mikhail Pak, Nathaniel J. Smith, Nikolai Nowaczyk, Nikolay Shebanov, Oleksandr Pavlyk, Per A. Brodtkorb, Perry Lee, Robert T. McGibbon, Roman Feldbauer, Sam Lewis, Sam Tygier, Scott Sievert, Sebastiano Vigna, Stefan Peterson, Surhud More, Tadeusz Pudlik, Takuya Oshima, Thomas J. Pingel, Thomas P. Robitaille, Thomas Spura, Thouis R. Jones, Tim Cera, Tim Leslie, Tiziano Zito, Tom Krauss, Utkarsh Upadhyay, Yaroslav O. Halchenko, and Yoshiki Vázquez-Baeza. SciPy 1.0: fundamental algorithms for scientific computing in Python. *Nat. Methods*, 17(3):261–272, 2020.

[22] Alexander C. Reis and Howard M. Salis. An automated model test system for systematic development and improvement of gene expression models. *ACS Synth. Biol.*, 9(11):3145–3156, 2020.

[23] Joseph P. Torella, Florian Lienert, Christian R. Boehm, Jan Hung Chen, Jeffrey C. Way, and Pamela A. Silver. Unique nucleotide sequence-guided assembly of repetitive DNA parts for synthetic biology applications. *Nat. Protoc.*, 9(9):2075–2089, 2014.

[24] Stefan De Kok, Leslie H. Stanton, Todd Slaby, Maxime Durot, Victor F. Holmes, Kedar G. Patel, Darren Platt, Elaine B. Shapland, Zach Serber, Jed Dean, Jack D. Newman, and Sunil S. Chandran. Rapid and reliable DNA assembly via ligase cycling reaction. *ACS Synth. Biol.*, 3(2):97–106, 2014.

[25] Daniel G. Gibson, Lei Young, Ray Yuan Chuang, J. Craig Venter, Clyde A. Hutchison, and Hamilton O. Smith. Enzymatic assembly of DNA molecules up to several hundred kilobases. *Nat. Methods*, 6(5):343–345, may 2009.

[26] Kaushik Raj, Naveen Venayak, Patrick Diep, Sai Akhil Golla, Alexander F. Yakunin, and Radhakrishnan Mahadevan. Automation assisted anaerobic phenotyping for metabolic engineering. *Microb. Cell Fact.*, 20(1):1–16, 2021.

[27] F. C. Neidhardt, P. L. Bloch, and D. F. Smith. Culture medium for enterobacteria. *J. Bacteriol.*, 119(3):736–747, 1974.

[28] Pandas Development team. pandas-dev/pandas: Pandas, feb 2020.

[29] Plotly Technologies Inc. Collaborative data science, 2015.

[30] Naveen Venayak, Kaushik Raj, and Radhakrishnan Mahadevan. Impact framework: A python package for writing data analysis workflows to interpret microbial physiology. *Metab. Eng. Commun.*, 9, 2019.

[31] Kathleen E. McGinness, Tania A. Baker, and Robert T. Sauer. Engineering Controllable Protein Degradation. *Mol. Cell*, 22(5):701–707, 2006.

[32] Stefan Klumpp, Zhongge Zhang, and Terence Hwa. Growth rate-dependent global effects on gene expression in bacteria. *Cell*, 139(7):1366–75, dec 2009.

[33] David W. Erickson, Severin J. Schink, Vadim Patsalo, James R. Williamson, Ulrich Gerland, and Terence Hwa. A global resource allocation strategy governs growth transition kinetics of Escherichia coli. *Nature*, 551(7678):119, nov 2017.

[34] F.C. Neidhardt. *Escherichia Coli and Salmonella: Cellular and Molecular Biology.* Number v. 1-2 in Escherichia Coli and Salmonella: Cellular and Molecular Biology. ASM Press, 1996.

[35] Jia Xu and Kathleen S. Matthews. Flexibility in the inducer binding region is crucial for allostery in the Escherichia coli lactose repressor. *Biochemistry*, 48(22):4988–4998, jun 2009.

[36] Subhayu Basu, Yoram Gerchman, Cynthia H. Collins, Frances H. Arnold, and Ron Weiss. A synthetic multicellular system for programmed pattern formation. *Nature*, 434(7037):1130–1134, apr 2005.

[37] Xiaoying Chen, Jennica L. Zaro, and Wei Chiang Shen. Fusion protein linkers: Property, design and functionality. *Adv. Drug Deliv. Rev.*, 65(10):1357–1369, 2013.

[38] Jianshen Hou, Cong Gao, Liang Guo, Jens Nielsen, Qiang Ding, Wenxiu Tang, Guipeng Hu, Xiulai Chen, and Liming Liu. Rewiring carbon flux in Escherichia coli using a bifunctional molecular switch. *Metab. Eng.*, 61:47–57, 2020.